POLITECNICO
MILANO 1863

SCUOLA DI INGEGNERIA INDUSTRIALE
E DELL'INFORMAZIONE

Executive Summary of the Thesis

Evaluation of Lunar GNSS- and Vision-Based Techniques for Lunar Landing

Laurea Magistrale in Space Engineering - Ingegneria Spaziale

Author: Elena Pilo

Advisor: Prof. Paolo Panicucci

Co-advisor: Prof. Francesco Topputo, Felice Piccolo

Academic year: 2022-2023

1. Introduction

Recent successful missions towards Earth's natural satellite have underscored its significance in space exploration, indicating that it will be in the spotlight for many years, with numerous upcoming missions already planned. The South Pole in particular, represents a region of great interest due to its high scientific potential. However space probes face challenges in precision landing, as evidenced by many mission failures, and continuous effort is performed to increase accuracy and reliability, in order to meet the stringent requirements identified by the ISECG 2019, aimed at landing with 90 m accuracy (3σ) on ground. State-of-the-art approaches see the exploitation of multiple electro-optical sensors to overcome the hurdles posed by such a challenging scenario, and to compensate the limitations of the respective technologies, resulting often in higher costs and power demand. To overcome these issues and enhance spacecrafts capabilities to navigate in real-time, space agencies like ESA and NASA proposed the development of a Lunar Communication and Navigation Service (LCNS), a constellation infrastructure around the Moon. Many studies are currently being carried out to assess the achievable level of performance of lunar GNSS [1], although this is usually considered as the primary or solely sensor. Therefore this thesis aims at exploring the potentialities of LCNS-based navigation while concurrently evaluating the outcome with a vision-based algorithm, providing a contribution to potential future integration of LCNS observables with other sensors like cameras. Thus the work is stems from the following main research question and sub-questions:

To what extent can lunar constellation measurements for absolute navigation enhance the accuracy of a Lunar landing, in comparison with Vision-Based Navigation techniques?

- *What is the optimal way of integrating constellation measurements inside a navigation filter?*
- *How does the accuracy change considering different constellations' configuration?*
- *What is the achievable accuracy during different phases of a descent scenario?*

2. Mission scenario

2.1. Landing trajectory

The considered mission scenario includes the coasting and braking phases of a Lunar landing aimed

at the South Pole. To simulate the ground-truth dynamics, the main perturbations acting on the spacecraft have been modelled. The Moon gravitational potential is modelled with a Spherical Harmonics expansion up to the 40th order and degree, to account for the irregularities of lunar gravity field. Additionally, also the contribution of Earth as third body is taken into account. Among the non-gravitational perturbations acting on the spacecraft, the SRP is modelled, considering a cannonball model.

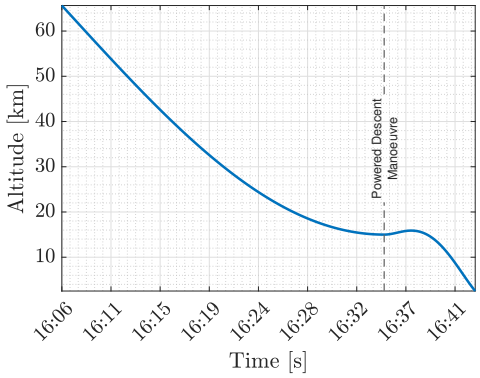

Figure 1: Altitude evolution

Coasting

The coasting arc is usually initiated with a Deorbiting Manoeuvre (DM) from a Low Lunar Orbit (LLO) set at 100 km altitude. This work focuses on the ultimate portion of this arc, namely from aruond 65 km altitude. This choice is mainly dictated by the availability of the LCNS satellites, as highlighted in fig. 3. In this phase all three above mentioned perturbations are included. Concerning the spacecraft attitude, during this phase, it is assumed to maintain Nadir pointing.

Braking

The braking phase spans from 15 km altitude up to 3 km ca. The spacecraft dynamics is expressed in the MCMF (Moon-Centered Moon-Fixed) frame, as it would ease the insertion of landmarks for future development, which would be conveniently represented by constant vectors. In this case, only the contribution of the spherical harmonics and the Earth is considered. The initial mass of the lander and its specific impulse are retrieved from [2] and are respectively $m_0 = 2822\ kg$ and $I_s = 309\ s$
A realistic attitude guidance is provided in this phase, also taken from [2]. The initial thrust angle is tilted of 5 deg with respect to the roll direction. Therefore the resulting thrust has also a vertical component, causing a slight elevation in the spacecraft's altitude, as depicted in the final phase of fig. 1.

2.2. LCNS Constellation

The selected LCNS constellation is retrieved from [1], as finding the optimal configuration is beyond the scope of this thesis. The LCNS satellites are positioned in three Elliptical Lunar Frozen Orbits as depicted in fig. 2.

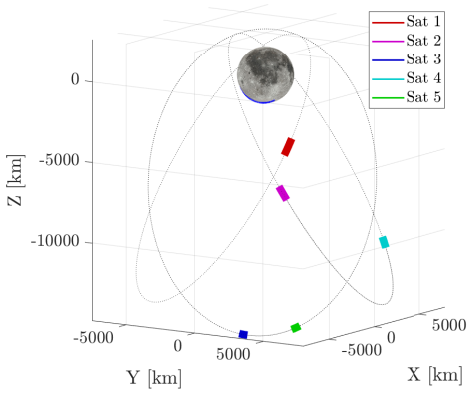

Figure 2: ELFO Constellation

All satellites within the constellation have the same semi-major axis (9750.7 km), eccentricity (0.7), inclination (63.2 deg) and argument of periapsis (90 deg), while the other right ascension and initial true anomaly are reported in table table 1.

Table 1: Constellation orbital parameters

	1	2	3	4	5
Ω $[deg]$	0	120	240	120	240
ϑ $[deg]$	0	164	196	245	184

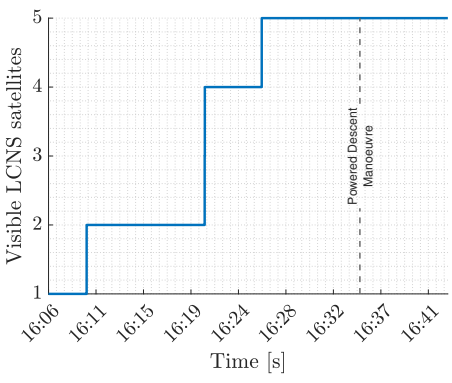

Figure 3: LCNS satellites during the descent

The orbits are propagated from this initial true anomaly to ensure full visibility during the braking phase, using a simple Two-Body Problem (TBP). Finally, the satellites' visibility during the whole considered trajectory is reported in fig. 3.

3. Sensors and observables

The lander sensor suite comprises an Inertial Measurement Unit (IMU), based on the LN200S, which includes an accelerometer and a gyroscope to provide data on thrust acceleration and angular velocity. Additionally, three sensors are employed to supply observables to be integrated in the filter: a LCNS receiver, a camera, and a Star tracker.

3.1. IMU

The acceleration and angular velocity acquired by the IMU are reported in eq. (1), considering the dynamics in the MCMF frame. Since the frame is not inertial but fixed to the Moon, the angular velocity includes the term related to Moon's rotations.

$$\begin{aligned} \boldsymbol{a}_{IMU} &= A_{B/MF}\left(\boldsymbol{a}_{thrust}\right) + \boldsymbol{b}_a + \boldsymbol{\eta}_a \\ \boldsymbol{\omega}_{IMU} &= \boldsymbol{\omega} + A_{B/MF}\boldsymbol{\omega}_{moon} + \boldsymbol{b}_g + \boldsymbol{\eta}_\omega \end{aligned} \tag{1}$$

Both values of $\boldsymbol{\eta}_\omega$ and $\boldsymbol{\eta}_a$, as well as the noises $\boldsymbol{\eta}_{b_g}$ and $\boldsymbol{\eta}_{b_a}$ driving the biases are assumed to be white Gaussian noises with standard deviations respectively equal to $\sigma_\omega = 0.07\ deg/\sqrt{h}$, $\sigma_a = 35\ \mu g/\sqrt{Hz}$ and $\sigma_{b_g} = 0.005\ deg/s^{\frac{3}{2}}$, $\sigma_{b_a} = 3\ \mu g/s^{\frac{3}{2}}$.

3.2. LCNS receiver

The LCNS receiver is considered to be analog to a GNSS receiver, thus implementing standard acquisition and tracking through which it provides measurements in terms of *pseudorange* and *pseudorange-rate*. To generate the real observables to be then fed to the navigation filter, their model can be simplified as reported in eq. (2):

$$\begin{aligned} \tilde{\rho}_i &= ||\tilde{\boldsymbol{r}}_i - \boldsymbol{r}|| + b_c + \varepsilon_{\rho_i} \\ \dot{\tilde{\rho}}_i &= \frac{(\tilde{\boldsymbol{r}}_i - \boldsymbol{r}) \cdot (\tilde{\boldsymbol{v}}_i - \boldsymbol{v})}{\rho_i} + d_c + \varepsilon_{\dot{\rho}_i} \end{aligned} \tag{2}$$

where $\boldsymbol{r}, \boldsymbol{v}$ and $\tilde{\boldsymbol{r}}_i, \tilde{\boldsymbol{v}}_i$ are respectively the user position and velocity, and the position end velocity of the i-th satellite within the constellation, transmitted within the broadcast navigation message to the user. The clock bias and drift are represented through b_c and d_c and are modelled according to a two-state clock model as:

$$\begin{aligned} \dot{b}_c &= d_c + \xi_{b_c} \\ \dot{d}_c &= \xi_{d_c} \end{aligned} \tag{3}$$

with ξ_{b_c} and ξ_{d_c} are two white Gaussian noises, whose stochastic parameters are retrieved from the Allan variance of the selected receiver clock. When broadcasting the signal to the user, the navigation message as well as the constellation ephemerides will contain errors, derived from the Orbit Determination (OD) and Time Synchronisation (TS) process. These errors are commonly encompassed in the definition of Signal In Space Errors (SISE). TS errors are taken into account in the white Gaussian terms ε_{ρ_i} and $\varepsilon_{\dot{\rho}_i}$ appearing in the measurement equation. OD errors instead enters directly in $\tilde{\boldsymbol{r}}_i$ and $\tilde{\boldsymbol{v}}_i$ as additive white Gaussian noises $\varepsilon_{r_i}, \varepsilon_{v_i}$. The standard deviations of these errors are reported in table 2

Table 2: GALILEO Signal In Space Error

Parameter	LCNS SISE (1σ)
Position ε_{r_i}	15 m ($3D$)
Velocity ε_{v_i}	0.15 m/s ($3D$)
Clock bias ε_{r_i}	10 m
Clock drift ε_{r_i}	0.1 m/s

The measurement noise covariance matrix is a diagonal matrix whose standard deviations are based on the errors affecting the code tracking loop and frequency tracking loop.

3.3. Camera

The lander is equipped with a monocular camera, that provides measurements in terms of the relative displacement of the spacecraft between two camera frames, which coincides with the two instants of the first and second image acquisition t_k and t_{k+m}. Therefore, the measurement model is a unit vector expressed in camera frame at the second time instant, as reported in eq. (4) [3].

$$^{\boldsymbol{C}}\boldsymbol{z}_{k+m} = \frac{A_{C/MF_{k+m}}\left({}^{MF}\hat{\boldsymbol{r}}^{-}_{k+m} - {}^{MF}\hat{\boldsymbol{r}}^{+}_{k}\right)}{||A_{C/MF_{k+m}}\left({}^{MF}\hat{\boldsymbol{r}}^{-}_{k+m} - {}^{MF}\hat{\boldsymbol{r}}^{+}_{k}\right)||} \tag{4}$$

Matrix $A_{C/MF}$ is the rotation matrix from the MCMF to the camera-fixed frame.

Since the measurement is a unit vector, its covariance will be a rank 2 matrix, built considering a motion direction error in the order of 1 *deg*, realistic for this type of measurements [4].

3.4. Star Tracker

The Star tracker provides measurements in terms of attitude angle error. Therefore the measurement equation to be fed to the filter is described as:

$$\delta\boldsymbol{\vartheta}_k = 2\frac{\left(\tilde{\boldsymbol{q}}_k \otimes \hat{\boldsymbol{q}}_k^{-1}\right)_{1:3}}{\left(\tilde{\boldsymbol{q}}_k \otimes \hat{\boldsymbol{q}}_k^{-1}\right)_4} \tag{5}$$

where $\hat{\boldsymbol{q}}_k$ is actually the predicted quaternion $\hat{\boldsymbol{q}}_k^-$ at time t_k, and $\tilde{\boldsymbol{q}}_k$ expresses the real attitude perturbed by white noise on each axis, whose standard deviation is equal to 10 *arcsec*.

4. Filtering schemes

Two filtering schemes are implemented within this work, processing either LCNS or camera observables. A visual representation is provided in fig. 4a and 4b. The first scheme employs a *tightly coupled* architecture to fuse the LCNS receiver with the IMU, being able to provide a navigation solution even with less than four visible satellites. The navigation filter estimates both translational and rotational motion of the spacecraft, as well as IMU and the receiver clock bias and drift. The full estimated state is thus:

$$\hat{\boldsymbol{x}} = [\hat{\boldsymbol{r}}^T, \hat{\boldsymbol{v}}^T, \hat{\boldsymbol{q}}^T, \hat{\boldsymbol{b}}_g^T, \hat{\boldsymbol{b}}_a^T, \hat{b}_c, \hat{d}_c]^T \tag{6}$$

The filter dynamics for the braking trajectory, written in the MCMF frame is reported in equation eq. (7). For the coasting arc the dynamics is instead expressed in the Moon-Centered-Inertial (MCI) frame and the terms accounting for the Moon's rotation as well as the thrust acceleration are not included, since no thrust is applied in this phase. The gravitational acceleration encompasses the contribution of J_2, the Moon's point gravity and Earth as third body.

$$\begin{aligned}
&\dot{\hat{\boldsymbol{r}}} = \hat{\boldsymbol{v}} \\
&\dot{\hat{\boldsymbol{v}}} = \hat{A}_{B/MF}^T\left(\tilde{\boldsymbol{a}}_{IMU}\right) - 2\left[\boldsymbol{\omega}_{Moon}\times\right]\hat{\boldsymbol{v}} \\
&\quad - \left[\boldsymbol{\omega}_{Moon}\times\right]^2\hat{\boldsymbol{r}} + \hat{\boldsymbol{a}}_g \\
&\dot{\hat{\boldsymbol{q}}} = \frac{1}{2}\Omega\left(\tilde{\boldsymbol{\omega}}_{IMU}\right)\hat{\boldsymbol{q}} \\
&\dot{\hat{\boldsymbol{b}}}_g = \boldsymbol{0} \qquad \dot{\hat{\boldsymbol{b}}}_a = \boldsymbol{0} \\
&\dot{\hat{b}}_c = \hat{d}_c \qquad \dot{\hat{d}}_c = 0
\end{aligned} \tag{7}$$

The term $A_{B/MF}$ is the rotation matrix from MCMF frame to body-fixed frame. The system of the estimated-state equations is integrated using an explicit 4th order Runge-Kutta integration scheme. The estimated IMU bias are used to correct the IMU measurements employed for the state propagation, while the clock bias and drift are directly inserted into the *pseudorange* and *pseudorange-rate* a-priori predictions.
Algorithm 1 reports the most important steps of the adopted algorithm for the absolute navigation scheme.

Algorithm 1 Error-State EKF

1: $\hat{\boldsymbol{x}}_k^- \leftarrow \dot{\hat{\boldsymbol{x}}} = \boldsymbol{f}(\hat{\boldsymbol{x}}_k$
2: $A_k = \left.\frac{\partial \boldsymbol{f}}{\partial \boldsymbol{x}}\right|_{\hat{\boldsymbol{x}}(t)}, H_k = \left.\frac{\partial \boldsymbol{h}}{\partial \boldsymbol{x}}\right|_{\hat{\boldsymbol{x}}_k}$
3: $P_k^- \leftarrow \dot{P} = AP + PA^T + Q^T$
4: $K_k = P_k^- H^T(H_k P_k^- H_k^T + R)^{-1}$
5: $\delta\hat{\boldsymbol{x}}_k^+ = K_k[\boldsymbol{y}_k - \boldsymbol{h}_k(\hat{\boldsymbol{x}}_k^-)]$
6: $\hat{\boldsymbol{x}}_k^+ = \hat{\boldsymbol{x}}_k^- + \delta\hat{\boldsymbol{x}}_k^+$
7: $P_k^+ = (I - K_k H_k)P_k^-(I - K_k H_k)^T + K_k R K_k^T$

The filter is designed to handle IMU measurements, and thus propagate the state, at a frequency of 10 Hz. In the absolute scheme the update occurs concurrently for the rotational and translational motion, at a frequency of 1 Hz. In the relative scheme instead, the attitude is still updated every second, yet the vision update occurs at a frequency of 0.1 Hz. This latter scheme is implemented based on the *stochastic cloning* algorithm [5]. Without entering into the details of the algorithm, the main idea consists in augmenting the filter state and covariance with a copy of the state, as soon as the first image is acquired. This necessity arises from the fact that when a measurement becomes available from the image processing, it does not only depend on the actual time instant, but rather on previous states, to which it must be somehow related. This concept is mathematically proved in [5]. Therefore, augmenting the state allows to take into account correlations between different time instants.
In this relative scheme, attitude is estimated concurrently, yet it is treated as a consider parameter, as highlighted in fig. 4b. This implies that the filter covariance encompasses also the error-angle covariance, although it remains unchanged within the vision algorithm update. Finally, the process noise matrix Q is considered as a tuning parameter in both cases.

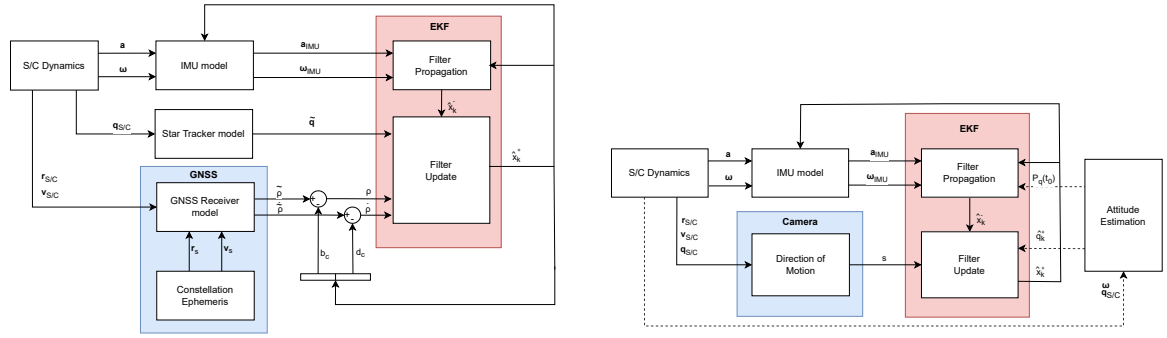

(a) Absolute navigation (b) Relative navigation

Figure 4: Navigation filter schemes

5. Braking

For the braking phase, initial position and velocity uncertainties are set equal to $\sigma_{r,0} = 100\,m(3D)$ and $\sigma_{v,0} = 10\ m/s(3D)$, which are conservative values compared to the achievable performance of the orbit determination process performed before the descent initiation thanks to the LCNS [1]. The initial uncertainties for the clock bias and drift are set equal to $\sigma_{b_c,0} = 100\ m$ and $\sigma_{d_c,0} = 1\ m/s$, while for the IMU the same values of σ_{b_g} and σ_{b_a} are used.

In fig. 5 the results obtained when all five satellites are visible are shown. It is evident that, given the measurements redundancy, the filter is able to estimate the state with errors even below 10 m in position and around 0.1 m/s in velocity. Navigation accuracy naturally degrades when fewer than five satellites are visible, with a worsening of the performance with only three satellites, as shown by the position error in fig. 6, due to lack of redundancy. This trend is also observed in velocity, where errors exceed 1 m/s. However, when fewer than 4 satellites are visible the ultimate performance can be improved by ensuring a proper geometry of the constellation, in order to decrease the dilution of precision (DOP). Consequently, errors in position are reduced to less than 100 m, while velocity errors set around 0.5 m/s. This underscores the ability of the tightly coupled filter architecture to deliver satisfactory performance even with fewer than four satellites.

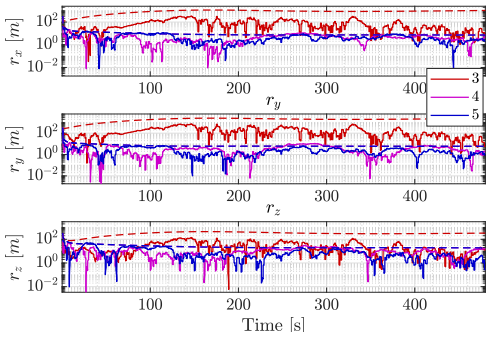

Figure 6: Position error with 3, 4 and 5 LCNS visible satellites

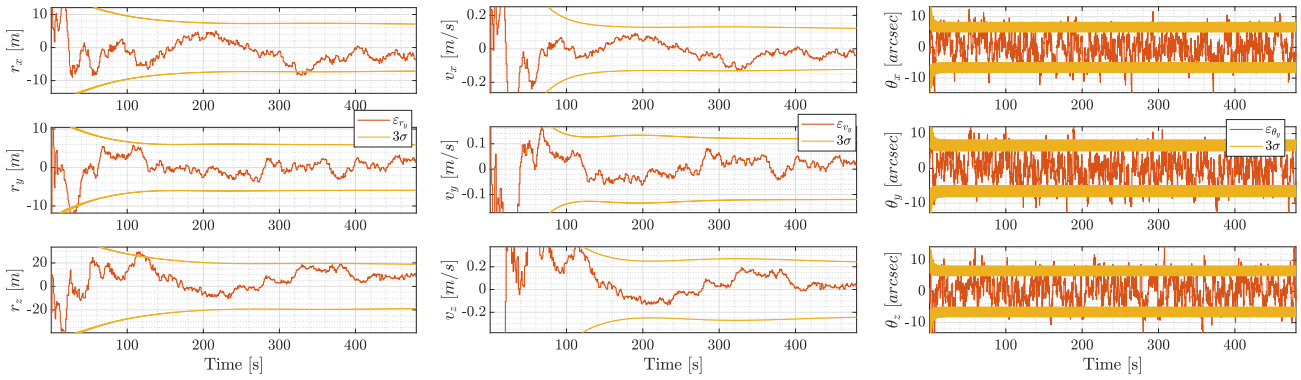

(a) Position error (b) Velocity error (c) Attitude error

Figure 5: Braking trajectory errors and 3σ bounds

6. Coasting

For the coasting arc the initial velocity uncertainty is lowered to 1 m/s, which is more in line with the achievable accuracy coming from OD, while the other values are unchanged. From figures 7a and 7b, showing the results obtained by the first navigation scheme during the coasting arc, is evident that in the initial part, when only one or two satellites are visible, the filter struggles to converge to an optimal solution, as not enough redundancy of the measurements is provided. However, as soon as four satellites come into view, the navigation solution sets to errors in line with the previous analysis. Employing the relative scheme, the implemented algorithm strives to reach acceptable levels of performance, as evident from the position error reported in fig. 7c, even if the velocity solution seems to converge. Nevertheless, if compared to the absolute scheme solution when only one or two satellites are visible, it seems able to mitigate the error-growth, reaching position errors below 500 m after 800 s ca. against the 1 km error obtained with the first navigation scheme.

7. Conclusions and future work

This thesis demonstrates that merging LCNS observables with an INS in a tightly coupled configuration yields accurate navigation solutions, even with fewer than 4 visible satellites, given proper constellation geometry. The stochastic cloning algorithm partially reduces propagation errors, yielding better solutions compared to scenarios with only one or two constellation satellites visible. While the algorithm alone may not produce satisfactory navigation solutions, it shows the potential for further enhancement and integration with the former filtering scheme. Adjusting the stochastic cloning algorithm, such as incorporating recent camera measurements into the state augmentation, could further improve its effectiveness. Additionally, integrating the full image processing pipeline and employing a more sophisticated model for the sensors could contribute to further refinement.

References

[1] A. Grenier, P. Giordano, *et al.*, "Positioning and velocity performance levels for a lunar lander using a dedicated lunar communication and navigation system," vol. 69, no. 2.

[2] S. Li, X. Jiang, and T. Tao, "Guidance Summary and Assessment of the Chang'e-3 Powered Descent and Landing," *Journal of Spacecraft and Rockets*, 2016.

[3] J. A. Christian, L. Hong, *et al.*, "Image-Based Lunar Terrain Relative Navigation Without a Map: Measurements," *Journal of Spacecraft and Rockets*, vol. 58, Jan. 2021.

[4] F. Piccolo, C. Balossi, *et al.*, "Resource-constrained vision-based relative navigation about small bodies," in *46th AAS Guidance, Navigation and Control Conference*, 2024.

[5] S. Roumeliotis and J. Burdick, "Stochastic cloning: a generalized framework for processing relative state measurements," in *Proceedings 2002 IEEE International Conference on Robotics and Automation*, May 2002.

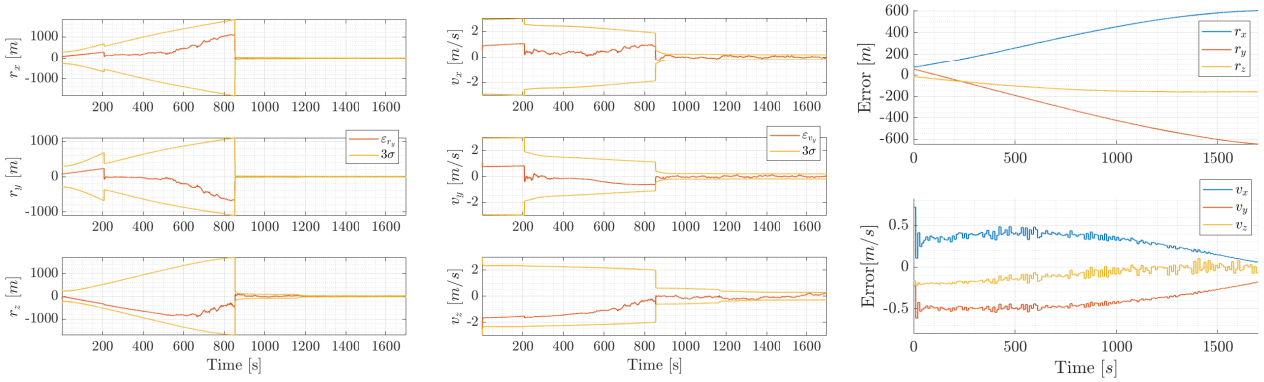

(a) Position error (b) Velocity error (c) Position and velocity error

Figure 7: Position and velocity errors and 3σ bounds for the absolute (a)-(b) and relative (c) scheme